SANDIA REPORT
SAND201X-XXXX
Unlimited Release
Printed Month and Year

Quantum Nanofabrication: Mechanisms and Fundamental Limits

George T. Wang, Michael E. Coltrin, Ping Lu, Philip R. Miller, Benjamin Leung, Xiaoyin Xiao, Keshab Sapkota, François Leonard, Gabriela Bran-Anleu, Daniel D. Koleske, Jeffrey Y. Tsao, Ganesh Balakrishnan, Sadhvikas Addamane, Jeffrey S. Nelson

Prepared by
Sandia National Laboratories
Albuquerque, New Mexico 87185 and Livermore, California 94550

Sandia National Laboratories is a multimission laboratory managed and operated by National Technology and Engineering Solutions of Sandia, LLC, a wholly owned subsidiary of Honeywell International, Inc., for the U.S. Department of Energy's National Nuclear Security Administration under contract DE-NA0003525.

Issued by Sandia National Laboratories, operated for the United States Department of Energy by National Technology and Engineering Solutions of Sandia, LLC.

Available to DOE and DOE contractors from

U.S. Department of Energy
Office of Scientific and Technical Information
P.O. Box 62
Oak Ridge, TN 37831

Telephone: (865) 576-8401
Facsimile: (865) 576-5728
E-Mail: reports@osti.gov
Online ordering: http://www.osti.gov/scitech

Available to the public from

U.S. Department of Commerce
National Technical Information Service
5301 Shawnee Rd
Alexandria, VA 22312

Telephone: (800) 553-6847
Facsimile: (703) 605-6900
E-Mail: orders@ntis.gov
Online order: https://classic.ntis.gov/help/order-methods/

SAND201X-XXXX
Printed September 2018
Unlimited Release

Quantum Nanofabrication: Mechanisms and Fundamental Limits

George T. Wang*, Michael E. Coltrin, Ping Lu, Philip R. Miller, Benjamin Leung, Xiaoyin Xiao, Keshab Sapkota, François Leonard, Gabriela Bran-Anleu, Daniel D. Koleske, Jeffrey Y. Tsao, Jeffrey S. Nelson
Sandia National Laboratories
P. O. Box 5800
Albuquerque, New Mexico 87185-MS1086
*e-mail : gtwang@sandia.gov

Ganesh Balakrishnan, Sadhvikas Addamane
Center for High Technology Materials, University of New Mexico
1313 Goddard St. SE
Albuquerque, New Mexico, 87106

Abstract

Quantum-size-controlled photoelectrochemical (QSC-PEC) etching, which uses quantum confinement effects to control size, can potentially enable the fabrication of epitaxial quantum nanostructures with unprecedented accuracy and precision across a wide range of materials systems. However, many open questions remain about this new technique, including its limitations and broader applicability. In this project, using an integrated experimental and theoretical modeling approach, we pursue a greater understanding of the time-dependent QSC-PEC etch process and to uncover the underlying mechanisms that determine its ultimate accuracy and precision. We also seek to broaden our understanding of the scope of its ultimate applicability in emerging nanostructures and nanodevices.

ACKNOWLEDGMENTS

We thank Arthur J. Fischer and G. Allen Vawter for helpful technical discussions and Ganesh Subramania and Anthony Coley for technical assistance with the PEC etch setup. This work was performed, in part, at the Center for Integrated Nanotechnologies, an Office of Science User Facility operated for the U.S. DOE, Office of Science. This work was supported by the Laboratory Directed Research and Development program at Sandia National Laboratories.

TABLE OF CONTENTS

FIGURES

TABLES

NOMENCLATURE

Abbreviation	Definition
Abbreviation	Definition
QSC	Quantum-Size-Controlled
PEC	Photoelectrochemical
STEM	Scanning Transmission Electron Microscopy
GaN	Gallium Nitride
InGaN	Indium Gallium Nitride
SEM	Scanning Electron Microscopy
PL	Photoluminescence
MQW	Multiple Quantum Well
MBE	Molecular Beam Epitaxy
NW	Nanowire
QD	Quantum Dot
AFM	Atomic Force Microscopy

1. INTRODUCTION

Semiconductor nanostructures exhibiting quantum-size effects represent the next frontier in nanophotonics and nanoelectronics, capable of enhanced performance and new functionalities. Semiconductor quantum nanostructures, which exhibit size-related quantum confinement effects, have unique electrical and optical properties that can enable future nanophotonics and nanoelectronics with superior performance and new and expanded functionalities. Quantum dot (QD)-based materials offer the potential for ultra efficient and low threshold lasers, ultrasensitive optical photodetectors, and on-demand single & entangled photon sources and detectors for quantum information systems[1-3]. Additionally, QD structures and devices exhibit superior radiation hardness compared to quantum wells (QWs), making them of interest for space and nuclear weapons applications[4-6]. However, the controlled fabrication of nanostructures in the ~sub-10 nm quantum size regime has proved extremely difficult using current approaches, limiting the potential of quantum nanostructure enabled devices.

Quantum size effects themselves can potentially be exploited to precisely control nanofabrication. By influencing the energies of electronic states, these effects will influence the susceptibility of the developing nanostructure to excitation by photons or electrons, and thus to material addition or subtraction processes mediated by excited electronic states. Recently, we demonstrated for the first time the ability to create epitaxial nanostructures using just such a process: quantum-size-controlled photoelectrochemical (QSC-PEC) etching [7]. PEC etching depends on light absorption, light absorption depends on bandgap, and bandgap depends on nanostructure size. QSC-PEC etching can thus *self-terminate* at a *wavelength-determined* size/bandgap. The principle is illustrated in Figure 1. *Sandia's pioneering work* has already enabled ~5X narrower InGaN quantum dot (QD) ensemble energy dispersion than typical of standard strain-driven QD growth.

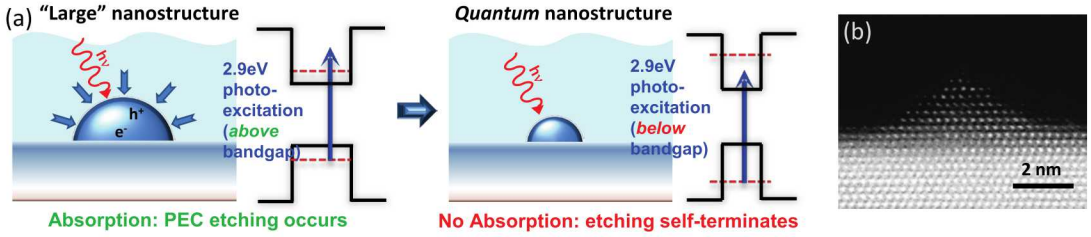

Figure 1. (a) Schematic illustrating principle of QSC-PEC etching; (b) InGaN QD on GaN film created by QSC-PEC etching

We believe that this new paradigm of "quantum nanofabrication" using quantum-size effects can potentially be the solution to the challenges of accuracy and precision in quantum nanostructure fabrication. Here, in this project, we propose a joint experimental and theoretical approach to elucidate the nature and fundamental mechanisms of QSC-PEC etching that determine its ultimate accuracy and precision. This will enable us to understand the scope of its ultimate applicability in emerging quantum nanostructures and nanodevices across a wider range of materials systems.

2. PROJECT GOALS

QSC-PEC etching can potentially be a game-changer in enabling the fabrication of epitaxial quantum nanostructures with unprecedented accuracy and precision across a wide range of materials systems. However, many open scientific and practical questions remain about this new technique, including its fundamental limitations and broader applicability. Using an integrated experimental and theoretical modeling approach, we thus propose here to pursue a detailed understanding of the time-dependent QSC-PEC etch process and to uncover the underlying mechanisms that determine its ultimate accuracy and precision in terms of size and bandgap uniformity, bandgap tunability, and placement. Achieving this will allow us to understand the scope of its ultimate applicability in emerging nanostructures and nanodevices across a broad range of disparate materials systems.

Some key goals of this work are listed below and described further in the Results and Accomplishments Section:

- Investigate time-dependent QSC-PEC etch processes and mechanisms
- Extend QSC-PEC etching to exemplary system: GaAs/AlGaAs
- Demonstrate controlled placement of QSC-PEC etched QDs
- Study surface passivation strategies
- Explore feasibility of QSC-PEC etching of 1D wires
- Modeling of PEC etching in nanostructures

3. EXPERIMENTAL PROCEDURES

Laser-Assisted Photoelectrochemical Etch Setup

For InGaN/GaN etching, the second harmonic of a tunable Ti:sapphire laser (400−500 nm wavelength, 2 ps pulse width, <1 nm line width, 82 MHz pulse repetition rate) was used for photoexcitation during PEC etching. Non-frequency doubled light (~780-830 nm) from the Ti:sapphire laser was used for GaAs PEC etching. Light was directed through an optical fiber, then a quartz window, and ~1.5 cm of electrolyte, before striking the sample. The samples were suspended in the PEC cell with PEC etching performed using a CH Instruments 660 electrochemical analyzer. As electrodes, we used a Pt counter electrode and an Ag/AgCl reference electrode from Bioanalytical Systems. The electrode potential was referenced to Ag/AgCl (3 M NaCl).

Scanning Transmission Electron Microscopy (STEM)

The TEM specimen was prepared by focus ion beam (FIB) with Ga ions. A final ion-milling step was carried out with 5 keV Ga ions at an incidence angle of 2° to reduce surface damage. An FEI Titan™ G2 80-200 STEM with a Cs probe corrector and ChemiSTEM™ technology (X-FEG™ and SuperX™ EDS with four windowless silicon drift detectors) operated at 200 kV was used for structural and chemical analysis. STEM images were typically recorded with a high-angle annular dark-field (HAADF) detector with a collection range of 60-160 mrad. For the energy-dispersive x-ray spectroscopy (EDS) data acquisition, the following parameters were typically used: electron probe size (FWHM) of about 0.13 nm, convergence angle of 18.1 mrad, and current of ~75 pA. The EDS spectral images used a Bruker software Esprit™ and were acquired as a series of frames, where the same region was scanned multiple times. Frames were spatially drift-corrected to build up spectral imaging dataset using a reference HAADF image. A total acquisition time of greater than 30 minutes was typically used.

Sample Preparation and PEC Etching Conditions

InGaN epilayers of thicknesses ranging from 3 to 20 nm were grown on ~5 μm thick Si-doped (n-type) c-plane GaN epilayers on sapphire substrates by metal-organic chemical vapor deposition (MOCVD). GaAs epilayers ranging from approximately 40-50 nm were grown by molecular beam epitaxy on AlGaAs epilayers grown on semi-insulating GaAs substrates. After the wafers were cut into ~1.5 cm × 0.5 cm pieces, indium metal contacts were applied as the working electrodes. For InGaN etching, H_2SO_4 aqueous solutions were typically used as the working electrolyte, as KOH has a finite etch rate for GaN. For pH studies, solution pH was varied by varying electrolyte composition: 0.2 M H_3PO_4 (pH 2.8), 0.2 M KOH (pH 13), and 0.2 M phosphate buffers (pH 5.2 and 11.4). The laser wavelength varied from 420-430 ± 1 nm, and its power was ~10 mW incident on a spot area ~1 cm^2. For GaAs etching, the laser wavelength was set to 830 nm with an etch power of ~ 100 mW and voltage of 0.1V. For GaAs etching, a 1:20 HCl:H_2O aqueous solution was employed, which was measured to have a dark

etch rate of GaAs of < 0.015 nm/min for etched GaAs pillars. Approximately 0.2-0.5 cm^2 of the sample film was immersed in the electrolyte solution. For some experiments, the area exposed to the electrolyte was limited to a ~3 mm spot by masking the sample with tape with pre-punched holes.

4. KEY RESULTS AND ACCOMPLISHMENTS

4.1. Influence of pH on the Quantum-Size-Controlled Photoelectrochemical Etching of InGaN Quantum Dots

The pH at which the PEC etching is performed and the coordination properties of the anions in the electrolyte potentially play important roles in controlling the viability of the overall process. In this study, these pH effects were investigated. Cyclic voltammetry (CV) and chronoamperometry (CA), both sensitive probes of the electrochemistry, were applied to determine the dynamics (rates versus electrode potential and time) of the QSC-PEC etch process for various electrolyte of different pH. High-resolution scanning transmission electron microscopy (STEM) was then used to characterize the resulting film microstructure. From these measurements, we conclude not only that the QSC-PEC etching of InGaN QDs is only viable at low pH (acidic solutions), but that the reason why it is not viable at higher pH has to do with is due to the formation of insoluble oxides. This study was published in Ref [8].

4.2. Time-dependent QSC-PEC etch processes and mechanisms

Time-dependent studies of the QSC-PEC etch processes were investigated to shed more light into the etch process from early to late stages. Such studies were intended to allow us to better understand the nature of the breakup of the InGaN film into islands or dots, how the density and size of the dots change over time, and whether QSC-PEC etching is truly self-terminating over long etch times.

4.2.1. Initial InGaN Film Breakup

Atomic force microscopy (AFM) images of an InGaN epilayer on a GaN epilayer before and after PEC etching reveal that the breakup of the InGaN epilayer is not random as was initially assumed. Instead, as seen in Figure 2, larger dots/islands are formed (Fig. 2b) along the atomic step edges present in the unetched InGaN layer (Fig 2a). This result not only reveals insights into the film breakup mechanism, but suggests a mechanism to potentially control the density or arrangement of QDs based on starting surface morphology. Future experiments, for example, may vary the offcut angle of the sapphire growth substrate, which changes the InGaN/GaN step edge density, to see if this impacts the resulting QD distribution after etching.

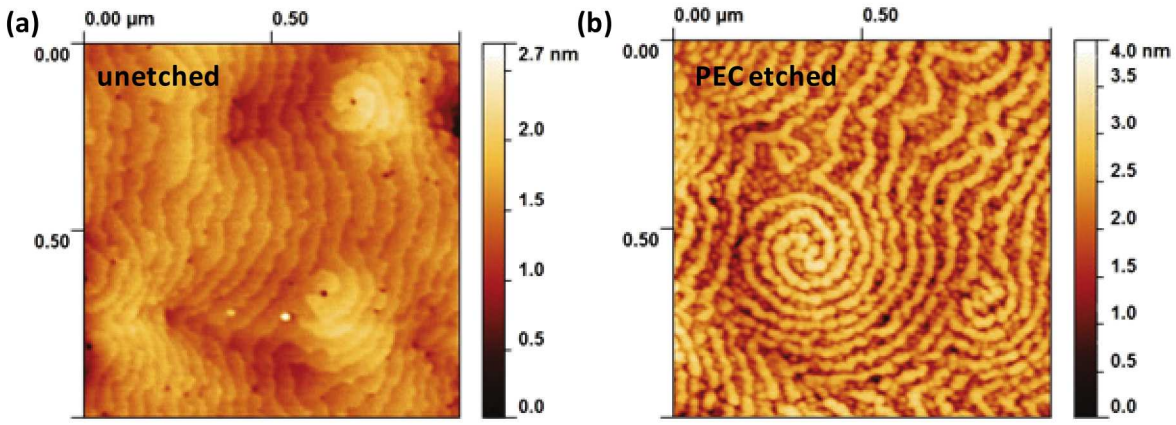

Figure 2.AFM images of (a) unetched InGaN film and (b) PEC etched InGaN film at 0.5V, showing dot nucleation along step edges

4.2.2. Time-dependent PEC etch studies of InGaN QDs

The time evolution of the InGaN QDs during etching was also investigated. Figure 3 shows the QD diameter and areal density for the same sample at three different etch times, which were estimated from analysis of AFM images. The results show that after initial breakup of the film into dense islands/dots, the dots continue to shrink in size with little change in dot density.

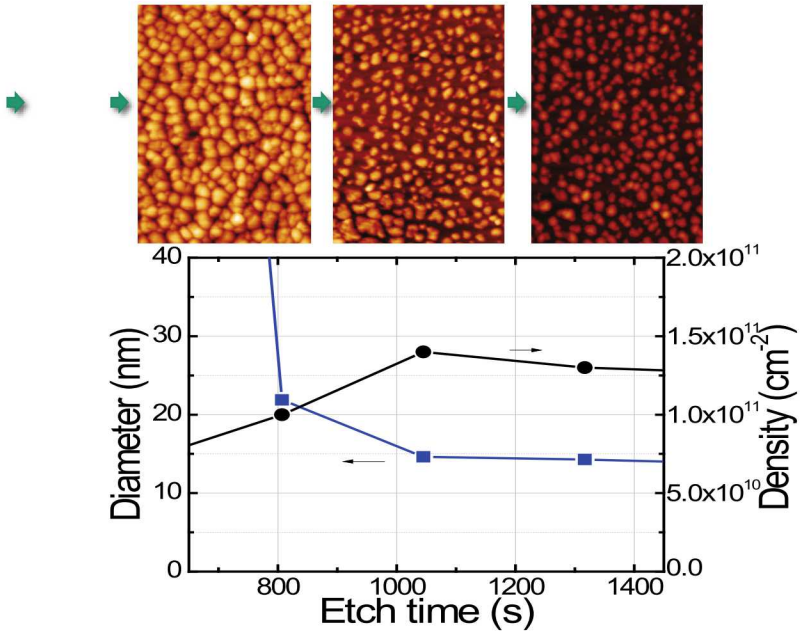

Figure 3. Dot diameter and density after 3 PEC etch times, along with AFM images

A time-dependent study with twelve PEC etch times (including zero etch time) was also conducted and the resulting QD peak wavelength emission and full-width half-max as measured by photoluminescence (PL) is plotted in Figure 4. It can be seen that the QD emission steadily blue-shifts with increasing etch time, indicating increasing bandgap and shrinking size, until around 4000s etch time. After this, the PL peak wavelength stabilizes, suggesting a termination of the PEC etch process, presumably due to quantum-size effects.

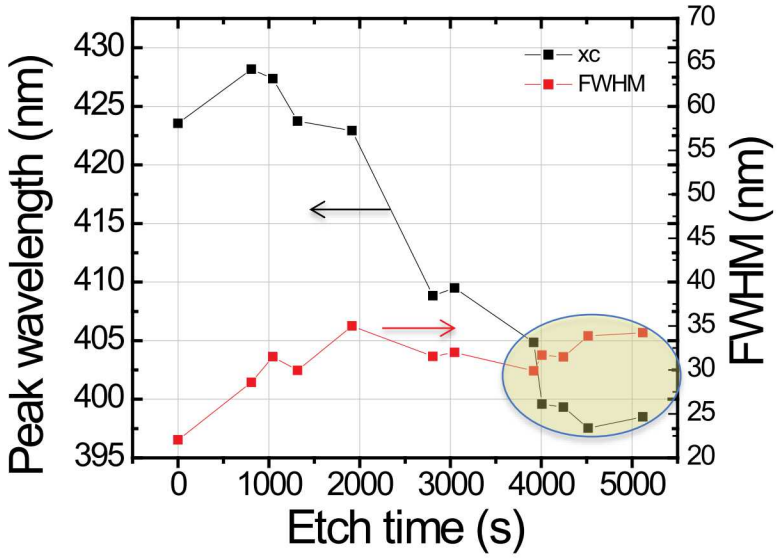

Figure 4. QD photoluminescence and FWHM as a function of PEC etch time

4.3. PEC Etching of Exemplary System: GaAs/AlGaAs

While AlGaInN-based QDs are desired for UV-visible nanophotonics, the III-nitrides have several characteristics, including high extended and point defect densities and strong internal polarization fields, that may obscure our fundamental understanding regarding the ultimate limits of QSC-PEC etching. Additionally, in ternary and quaternary alloys, such as InGaN, random alloy fluctuations exist[9], which not only impact their electrical and optical properties, but can result in compositional variations across QDs. As bandgap depends on composition, this obscures whether and to what degree observed QD size dispersions after QSC-PEC etching are from compositional fluctuations or arise from other factors.

In contrast to the III-nitrides, (Al)GaAs is grown on native GaAs substrates and enjoys near ideal lattice match for all compositions, resulting in extremely low dislocation densities several orders of magnitude lower ($<10^4$ cm^{-2} vs. mid-10^8 cm^{-2} for III-nitrides), and impurity incorporation in GaAs epilayers can be as low as 10^{12} cm^{-3} compared to ~10^{16} cm^{-3} for III-nitrides.[10] Additionally, as a binary system, any effects of compositional fluctuations on QSC-PEC etching are eliminated. The larger Bohr exciton radius, below which significant quantum-size effects occur, of GaAs (~12 nm vs. ~3 nm for GaN) will allow for much wider QD size

and bandgap tuning range to study the QSC-PEC process and facilitate structural characterization. *Thus, we propose that GaAs will serve as a near-ideal model system for probing the ultimate limits of QSC-PEC etching on size and bandgap specificity and uniformity*.

A series of PEC etching experiments were conducted on ~50 nm thick n-type GaAs epilayers (typical doping of 1e17 cm^{-2}) grown on a thick (typically ~ 1 µm) $Al_{0.39}Ga_{0.61}As$ layer on semi-insulating GaAs substrates by molecular beam epitaxy (MBE). The AlGaAs layer is intended to serve as the etch stop layer for the GaAs QDs to form on and to also prevent diffusion of unwanted holes to the top surface being etched[11]; these holes could potentially be generated in the underlying GaAs substrate by the UV laser, if it is able to penetrate the AlGaAs layer, and if they reach the top surface, could serve as an unlimited source of holes for GaAs dissolution which would prevent the QSC mechanism from taking place. We observed that at longer etching times, the top n-GaAs epilayer was completely etched away, as shown by cross-sectional scanning transmission electron microscopy (STEM) leaving no QDs. Because higher Al concentrations can potentially lead to higher wet etch susceptibility, a new set of samples were grown with the Al content reduced to 0.2 (Ga = 0.8). Figure 5 shows cross-sectional STEM images of the unetched sample and after 180 s and 480 s of PEC etching.

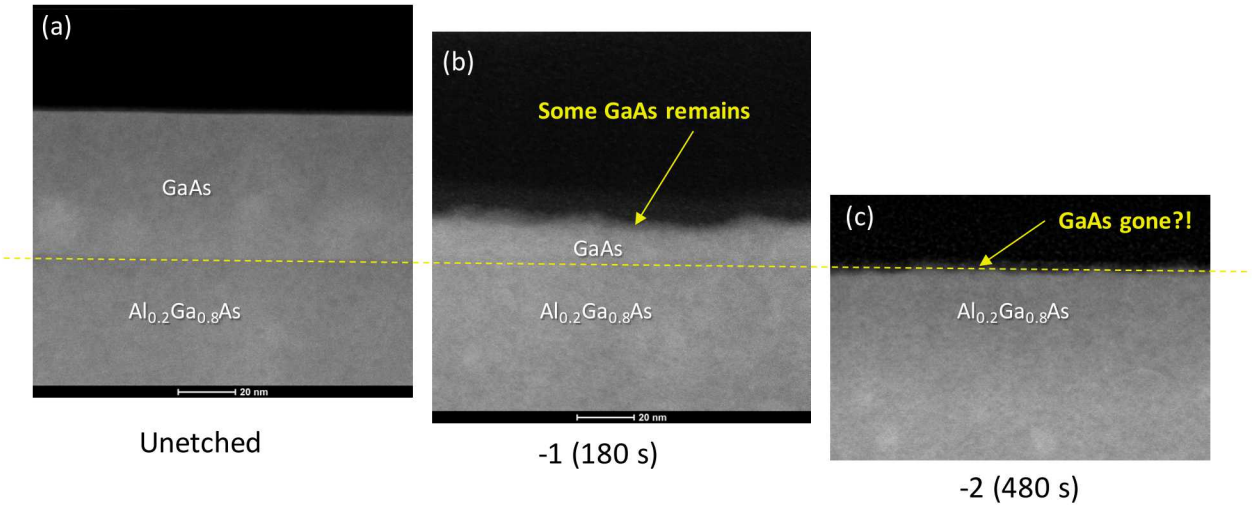

Figure 5.Cross-sectional STEM images of (a) unetched n-GaAs epilayer; (b) after 180 s etching; (c) after 480 s etching. Dotted yellow line indicates GaAs/AlGaAs interface (assumed in (c) for no AlGaAs etching).

Following 180 s of PEC etching, etching of the top n-GaAs epilayer is evident, with a thin layer of GaAs remaining. However, after 480 s of etching, no n-GaAs is seen, indicating its complete removal. This is in contrast to our QSC-PEC etching of InGaN on GaN, where InGaN QDs remained even at longer etching times due to the self-terminating etch. We hypothesis some potential reasons as to the lack of GaAs QD formation. The first is that the QSC-PEC etch process is defect-mediated or depends on the surface structure (e.g. step edge nucleation) that is not present for the GaAs/AlGaAs films etched here. The 830 nm wavelength laser used may also be too far above the GaAs bandgap at room temperature, leading to overetching. Finally, the AlGaAs layer may have a non-zero etch rate during the PEC etch

process. This is evidenced by cross-sectional SEM images showing sidewall roughness of the AlGaAs layer after PEC etching. Unwanted AlGaAs etching would also lead to the removal of any GaAs QDs that were formed on top during the QSC-PEC etch process. Future work will need to address these potential issues.

4.4. PEC Etching of QD Multilayers

While uncapped and capped single-layer InGaN QDs have been demonstrated by this QSC-PEC etching[7,12], devices requiring intense optical emission and high gain, such as QD-based lasers, would benefit from multiple layers of QDs, analogous to the multi-quantum well (MQW) structure of semiconductor LEDs and lasers. We performed PEC etching experiments on InGaN/GaN MQW structures with the goal of turning the quantum wells into multiple layers of quantum dots via QSC-PEC etching. The etch was performed at a wavelength of 420 nm in 0.2M H_2SO_4 for 45 minutes. A cross-sectional STEM image is shown in Figure 6. Despite the fact that the GaN barriers should serve as etch stops as their bandgap (~365 nm) is above the laser light used for PEC etching, it is seen that etching of all five InGaN QWs has been achieved. It is possible that etching of the InGaN QWs may proceed through the voids shown in Fig. X, which may be related to defects in the GaN layers that are PEC etched, providing a pathway for the etch solution to reach the underlying InGaN QW. Higher resolution STEM images show InGaN QDs in each InGaN layer with lateral dimensions around 2-3 nm along with some unetched InGaN QW regions. While this represents a promising initial result for creating multiple layers of QDs by QSC-PEC etching, which are passivated by GaN barriers on the top and bottom, future work will need to focus on better understand the etching process through the GaN barriers to maximize the QD density in each InGaN QW layer.

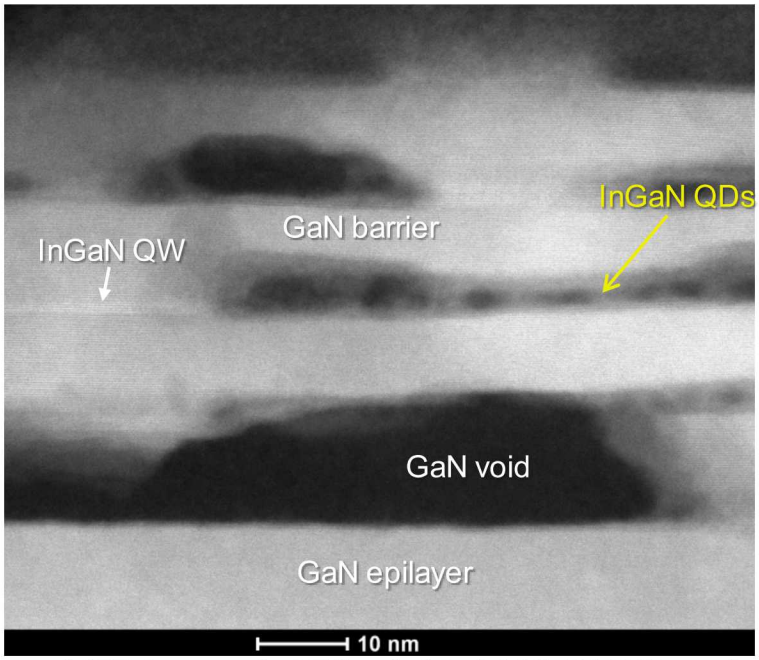

Figure 6. Cross-sectional STEM image of a PEC-etched InGaN/GaN MQW sample, showing multiple layers of InGaN QD formation.

4.5. Modeling of PEC Etching in Nanostructures

In this work we seek to understand the impact of nanostructure dimensions and geometry (e.g. nanofins, nanowires, nanodots) on the rate of photoelectrochemical etching by theoretical modeling, which to our knowledge remains relatively unexplored. To this end, a numerical approach that simulates all the transport process inside the semiconductor was developed. The approach is self-consistent between the electrostatic potential and carrier distribution. The problem is non-equilibrium due to the illumination.

4.5.1. Differential Equations

Poisson's equation is used to calculate the electric potential,

$\nabla \cdot (-\epsilon_r \nabla V) = q(p - n + N_d)$	Equation 1

where ϵ_r is the relative permittivity, V is the electrostatic potential, N_d is the donor concentration for complete doping ionization, and q is the electron charge. p and n are the hole and current densities, determined from the continuity equations,

$\nabla \mathbf{J}_\mathrm{p} = g_\mathrm{p} + r_\mathrm{p}$	Equation 2
$\nabla \mathbf{J}_n = r_\mathrm{p}$	Equation 3

where g_p represents the hole generation rate, and r_p and r_n represents the hole and electron recombination rates, respectively. $\mathbf{J}_p$ and $\mathbf{J}_n$ are the hole and electron current densities, and they are defined as

$\boldsymbol{J}_p = qp\mu_p \boldsymbol{E} - \mu_p k_b T \nabla p$	Equation 4
$\boldsymbol{J}_n = qp\mu_n \boldsymbol{E} + \mu_n k_b T \nabla n$	Equation 5

where μ_p and μ_n are the hole and electron mobility, k_b is the Boltzmann constant, and T is the temperature of the semiconductor. The electric field $\boldsymbol{E} = \nabla V$.

The hole generation rate g_p resulting from the absorption of the light can be calculated with the following expression,

$g_p = \frac{\alpha I_0}{h\nu} e^{-\alpha(R-r)}$	Equation 6

where α is the absorption coefficient, I_0 is the average intensity transmitted into the semiconductor at the surface, and $h\nu$ is the photon energy at the specific wavelength. The Shockley-Read-Hall Recombination Model [13,14] was used to calculate the electron recombination rate r_p,

$$r_n = r_p = \frac{np - n_{i,eff}^2}{\tau_p\left(n + n_{i,eff}\right) + \tau_n\left(p + n_{i,eff}\right)}$$ $$n_{i,eff} = \sqrt{N_c N_v} exp\left(-\frac{E_{g,0}}{2k_B T}\right)$$	Equation 2

where τ_p and τ_n are the hole and electron lifetime, N_c and N_v are the effective densities of states for the conduction and valence band, k_B is the Boltzmann's constant, and T is the temperature of the semiconductor.

4.5.2. Boundary Conditions

Ostermayer et. al. [15] assumed that the rate of dissolution of the semiconductor is proportional to the hole concentration at the semiconductor-electrolyte interface. Surface recombination and recombination close to the surface are neglected, so the normal component of the hole current at the interface is proportional to the rate of dissolution. Therefore, the boundary condition at the surface is

$\boldsymbol{J}_p \cdot \boldsymbol{n} = -qKp$	Equation 3
$\boldsymbol{J}_n \cdot \boldsymbol{n} = 0$	Equation 4

where K is the dissolution reaction velocity, and has the dimensions of velocity. The electric potential at the surface is

$V = V_o$	Equation 5

Where V_o is a constant value. It is chosen such that the Fermi level at equilibrium is located at the midgap of the semiconductor, since this is typical for Fermi level pinning at surfaces.

4.5.3. Numerical Model

A steady state numerical model was developed to calculate the spatial variation of the electric potential V, hole concentration p, and the electron concentration n in a GaAs n-type semiconductor. The model includes the effects of the hole photogeneration, diffusion, drift, and recombination in the semiconductor domain, and the hole reaction velocity for the decomposition at the surface of the semiconductor that is in contact with the electrolyte. The commercial software COMSOL [16] was used to solve for the electric potential and for the electron and hole concentrations. The finite volume method was used to discretize the set of coupled partial differential equations. The corresponding initial and boundary conditions were applied. The material properties used for the GaAs semiconductor are listed in Table 1. The parameters used to calculate the hole generation rate are listed in Table 2.

4.5.4. Parameters for Numerical Model

Table 1: Material Properties of GaAs

Variable	Symbol	Value
Relative permittivity	ϵ_r	12.9
Bang gap	$E_{g,0}$	1.424 V
Electron affinity	χ_0	4.07 V
Effective density of state, valence band	N_v	9.509E24 m^{-3}
Effective density of state, conduction band	N_c	4.209 E23 m^{-3}
Electron mobility	μ_n	0.85 m^2/ V-s
Hole mobility	μ_p	0.04 m^2/ V-s
Electron lifetime	τ_n	1.42E-09 s
Hole lifetime	τ_p	1.42E-09 s
Donor Concentration	N_d	5E21 m^{-3}

Table 2: Hole generation rate parameters

Variable	Symbol	Value
Average intensity	I_0	1000 W/m^2
Absorption coefficient	α	1E6 m^{-1}
Wavelength	λ	830 nm

4.5.5. Modeling Results

Figure 7 shows the band-bending inside nanowires of different diameters. As the diameter gets smaller, the electric potential is flatter, which decreases the driving force for holes to reach the surface (r* = 1). The impact is seen in Figure 8, where the hole concentration is seen to be flatter for smaller nanowire radii.

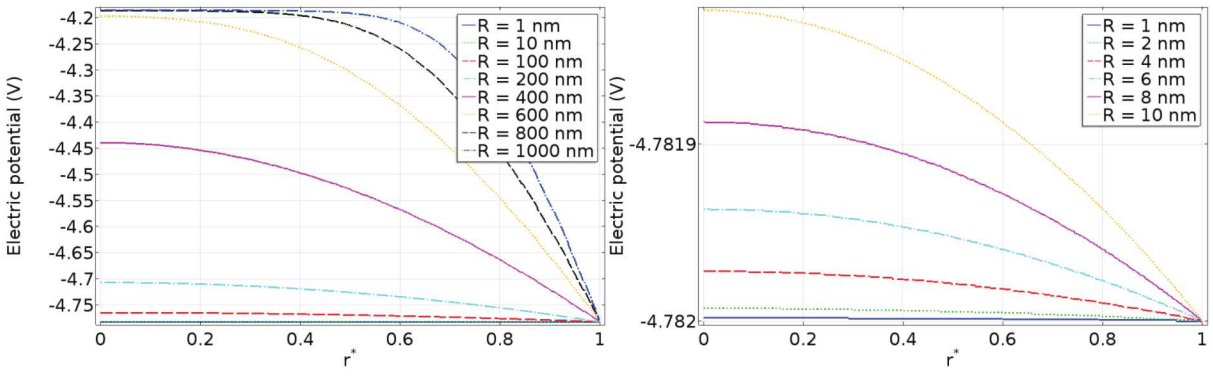

Figure 7. Calculated electrostatic potential as a function of position for different nanowire diameters. As the diameter gets smaller, the band-bending is flatter. r=r/R.*

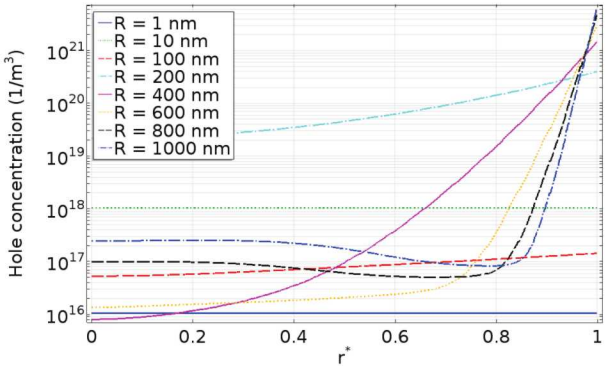

Figure 8. Calculated hole concentration inside nanowires of different diameters. r=r/R.*

The dissolution rate during etching is proportional to the hole concentration at the surface, both of which are plotted in Figure 9 as a function of diameter. Clearly the dissolution rate decreases by several orders of magnitude as the nanowire diameter is reduced.

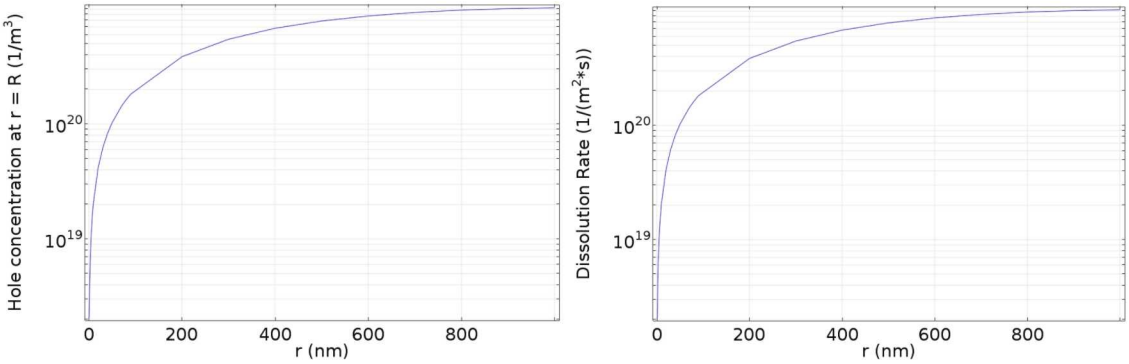

Figure 9. Left: Calculated hole concentration at the surface as a function of nanowire diameter. Right: Calculated dissolution rate as a function of nanowire diameter.

In summary, we developed a numerical approach that solves the coupled, non-equilibrium transport equations in the semiconductor during photoelectrochemical etching. Initial results indicate that the approach is viable, but more work is needed to address numerical issues (convergence in COMSOL) as well as understand the key physics that governs the PEC.

5. CONCLUSIONS

In conclusion, over the course of this project we attempted to better understand the fundamental mechanisms of quantum-size controlled (QSC-PEC) PEC etching and to extend its scope. Accomplishments include detailing the QSC-PEC etch process of InGaN over time, which revealed that the initial InGaN film breakup is related to the surface step/terrace morphology, and strong evidence that the process is indeed self-limiting. Successful etching of multiple layers of InGaN QDs from an InGaN/GaN MQW structure was also demonstrated, which may help open a route to QD-based optoelectronic devices including LEDs and lasers via this approach. A theoretical modeling framework for understand PEC etching in nanostructures, with nanofin or nanowire geometries, was also developed. The modeling results reveal that PEC etch rate can decrease by several orders of magnitude as the nanostructure size is reduced, due to surface band-bending effects. Our goal of extending QSC-PEC etching to other materials systems, such as GaAs/AlGaAs, as explored here, remains unfinished. Outstanding scientific and technical issues remain before the question can be definitely answered as to whether QSC-PEC etching is generally applicable to multiple materials systems. Overall, we remain optimistic that using quantum-size effects to control nanostructure formation will be increasingly explored and utilized in the future.

REFERENCES

1 Bimberg, D. & Pohl, U. W. Quantum dots: promises and accomplishments. *Materials Today* **14**, 388-397 (2011).

2 Chow, W. W., Lorke, M. & Jahnke, F. Will Quantum Dots Replace Quantum Wells As the Active Medium of Choice in Future Semiconductor Lasers? *Selected Topics in Quantum Electronics, IEEE Journal of* **17**, 1349-1355 (2011).

3 Lao, Y.-F., Wolde, S., Perera, A. U., Zhang, Y., Wang, T., Liu, H., Kim, J., Schuler-Sandy, T., Tian, Z.-B. & Krishna, S. InAs/GaAs p-type quantum dot infrared photodetector with higher efficiency. *Applied Physics Letters* **103**, 241115 (2013).

4 Ohshima, T., Sato, S.-i., Imaizumi, M., Sugaya, T. & Niki, S. in *Photovoltaic Specialists Conference (PVSC), 2011 37th IEEE.* 001605-001609 (IEEE).

5 Guffarth, F., Heitz, R., Geller, M., Kapteyn, C., Born, H., Sellin, R., Hoffmann, A., Bimberg, D., Sobolev, N. & Carmo, M. Radiation hardness of InGaAs/GaAs quantum dots. *Applied physics letters* **82**, 1941-1943 (2003).

6 Piva, P., Goldberg, R., Mitchell, I., Labrie, D., Leon, R., Charbonneau, S., Wasilewski, Z. & Fafard, S. Enhanced degradation resistance of quantum dot lasers to radiation damage. *Applied Physics Letters* **77**, 624-626 (2000).

7 Xiao, X., Fischer, A. J., Wang, G. T., Lu, P., Koleske, D. D., Coltrin, M. E., Wright, J. B., Liu, S., Brener, I. & Subramania, G. S. Quantum-Size-Controlled Photoelectrochemical Fabrication of Epitaxial InGaN Quantum Dots. *Nano Lett.* **14**, 5616-5620 (2014).

8 Xiao, X., Lu, P., Fischer, A. J., Coltrin, M. E., Wang, G. T., Koleske, D. D. & Tsao, J. Y. Influence of pH on the Quantum-Size-Controlled Photoelectrochemical Etching of Epitaxial InGaN Quantum Dots. *The Journal of Physical Chemistry C* **119**, 28194-28198, doi:10.1021/acs.jpcc.5b09555 (2015).

9 Schubert, E., Göbel, E., Horikoshi, Y., Ploog, K. & Queisser, H. Alloy broadening in photoluminescence spectra of Al x Ga 1-x As. *Phys. Rev. B* **30**, 813 (1984).

10 Manfra, M. J. Molecular Beam Epitaxy of Ultra-High-Quality AlGaAs/GaAs Heterostructures: Enabling Physics in Low-Dimensional Electronic Systems. *Annu. Rev. Condens. Matter Phys.* **5**, 347-373 (2014).

11 Khare, R., Young, D. B., Snider, G. L. & Hu, E. L. Effect of band structure on etch-stop layers in the photoelectrochemical etching of GaAs/AlGaAs semiconductor structures. *Appl. Phys. Lett.* **62**, 1809-1811, doi:10.1063/1.109556 (1993).

12 Xiao, X., Fischer, A. J., Coltrin, M. E., Lu, P., Koleske, D. D., Wang, G. T., Polsky, R. & Tsao, J. Y. Photoelectrochemical etching of epitaxial InGaN thin films: self-limited kinetics and nanostructuring. *Electrochim. Acta* **162**, 163-168 (2015).

13 Hall, R. N. Electron-hole recombination in germanium. *Physical review* **87**, 387 (1952).

14 Shockley, W. & Read Jr, W. Statistics of the recombinations of holes and electrons. *Physical review* **87**, 835 (1952).

15 Ostermayer Jr, F., Kohl, P. & Lum, R. Hole transport equation analysis of photoelectrochemical etching resolution. *Journal of applied physics* **58**, 4390-4396 (1985).

16 Multiphysics, C. User's guide. *Version* **4**, 290-298 (2007).

APPENDIX A: PUBLICATIONS, PATENTS, AND INVITED PRESENTATIONS RESULTING FROM THIS WORK

PATENTS

- Patent issued: "Quantum-size-controlled photoelectrochemical etching of semiconductor nanostructures, US 9,276,382 B2, Mar. 1, 2016

PUBLICATIONS (IN PREPARATION OR REVIEW)

- Xiao, X., P. Lu, A. J. Fischer, M. E. Coltrin, G. T. Wang, D. D. Koleske, J. Y. Tsao, *Influence of pH on the Quantum-Size-Controlled Photoelectrochemical Etching of Epitaxial InGaN Quantum Dots,* J. Phys. Chem. C, **119**, 28194 (2015).
- Addamane, S. J., A. Mansoori, N. Dawson, D.M. Shima, C.P. Hains, L.R. Dawson, G. T. Wang and G. Balakrishnan, *Photoluminescence-based comparison of optical properties of Stranski-Krastanov (S-K) InAs/GaAs quantum dots and InAs/InP quantum dashes*, Appl. Phys. Lett., in review
- G. T. Wang et al., "Fabrication of High Density, High Aspect Ratio Vertical GaN Nanowires by Photoelectrochemical Etching,," in preparation

INVITED PRESENTATIONS

- George T. Wang et al., "Top-down Fabrication for III-Nitride Nanophotonics," 2017 IEEE Photonics Society Summer Topicals Meeting, San Juan, Puerto Rico, July 10-12, 2017. (invited)
- George T. Wang**,** B. Leung, M.-C. Tsai, C. Li, G. Balakrishnan, et al., "Nanowires, Nanosheets, and Beyond: Three-Dimensional, High Aspect Ratio Nanostructures by Top-Down Etching of GaN," ICNS-12 Conference, 7/24-28/17, Strasbourg, France (invited).
- George T. Wang, Leung, B., M.-C. Tsai, C. Li, G. Balakrishnan, et al., "Top-Down Etching of Three-Dimensional, High Aspect Ratio GaN Nanostructures," 18th US Workshop on Organometallic Vapor Phase Epitaxy (OMVPE-18), 7/30-8/4/17, Santa Fe, NM (invited).
- George T. Wang, "III-Nitride nanostructures for photonics and beyond," 255th ACS National Meeting, 3/18-21/18, New Orleans, LA. (invited)
- George T. Wang, Leung, B., M.-C. Tsai, C. Li, G. Balakrishnan, et al., "Top-Down Etching of GaN Nanostructures for Optoelectronics and Beyond," SPIE Optics + Photonics Conference, 8/6-10/17, San Diego, CA (invited).

DISTRIBUTION

1	MS0892	Philip R. Miller	08634
1	MS1086	George T. Wang	01876
1	MS1086	Keshab Sapkota	01876
1	MS1411	Ping Lu	01819
1	MS1421	Jeffrey S. Nelson	01870
1	MS1421	Jeffrey Y. Tsao	01870
1	MS9161	François Leonard	08342
1	MS9957	Gabriela Bran-Anleu	08253
1	MS0899	Technical Library	9536 (electronic copy)
1	MS0359	D. Chavez, LDRD Office	1911

Sandia National Laboratories